Laser-driven Rayleigh-Taylor instability: Plasmonic effects and three-dimensional structures

A. Sgattoni,[1,2,*] S. Sinigardi,[1,3,4] L. Fedeli,[1,5] F. Pegoraro,[1,5] and A. Macchi[1,5,†]

[1]*Istituto Nazionale di Ottica, Consiglio Nazionale delle Ricerche, research unit Adriano Gozzini, Pisa, Italy*

[2]*Dipartimento di Energia, Politecnico di Milano, Milano, Italy*

[3]*Dipartimento di Fisica e Astronomia, Università di Bologna, via Irnerio 46, 40126 Bologna, Italy*

[4]*INFN sezione di Bologna, viale Berti Pichat 6/2, 40127 Bologna, Italy*

[5]*Dipartimento di Fisica Enrico Fermi, Università di Pisa, Largo Bruno Pontecorvo 3, I-56127 Pisa, Italy*

(Received 26 June 2014; published 21 January 2015)

The acceleration of dense targets driven by the radiation pressure of high-intensity lasers leads to a Rayleigh-Taylor instability (RTI) with rippling of the interaction surface. Using a simple model it is shown that the self-consistent modulation of the radiation pressure caused by a sinusoidal rippling affects substantially the wave vector spectrum of the RTI, depending on the laser polarization. The plasmonic enhancement of the local field when the rippling period is close to a laser wavelength sets the dominant RTI scale. The nonlinear evolution is investigated by three-dimensional simulations, which show the formation of stable structures with "wallpaper" symmetry.

DOI: 10.1103/PhysRevE.91.013106 PACS number(s): 52.38.Kd, 42.25.Gy, 47.20.Ma, 52.35.Py

I. INTRODUCTION

The Rayleigh-Taylor instability (RTI) is the classical process occurring when a heavy fluid stands over a lighter one in hydrodynamics or, equivalently, when a light fluid accelerates a heavier one. The latter case is of crucial importance in inertial confinement fusion [1] and in the astrophysical context, as exemplified in a spectacular way by the Hubble Space Telescope images of the Crab Nebula [2]. A peculiar example of the RTI arises in the context of ultraintense laser-plasma interactions where the radiation pressure of the laser pulse is large enough to drive a strong acceleration of a dense plasma target. Surface rippling attributed to RTI-like phenomena has been observed in simulations since early investigations of the ultraintense regime [3] and in several studies devoted to the concept of radiation pressure acceleration of thin targets [4–8], i.e., the "light sail" scheme which is being extensively studied experimentally [9,10] as one of the most promising approaches to laser-plasma acceleration of ions [11] especially at intensities beyond 10^{23} W cm^{-2} (foreseen with next-generation laser facilities), i.e., in the regime where the ions become relativistic and high energy gain is predicted [12–15]. The RTI may cause early breakthrough of the laser pulse through the thin foil target, leading to inefficient acceleration. Some experimental evidence of radiation-pressure-driven RTI in thin targets has been reported [10].

Analytical modeling of the laser-driven RTI of a thin foil in the ultraintense regime [4,8] predicts that the instability growth rate γ_{RT} increases monotonically with the wave vector q, similarly to the classic result for the hydrodynamic instability $\gamma_{\mathrm{RT}} = (gq)^{1/2}$, where g is the acceleration, thus apparently favoring the generation of small scales. However, simulations show that the size of the structures generated by the instability is finite and close to the laser wavelength [4,7,8].

In this paper, in order to explain the dominant spatial scales in the observed structures, we consider the effect of the transverse modulation of the radiation pressure caused by the rippling of the laser-plasma interface. By studying the reflection of a plane monochromatic wave by a shallow sinusoidal grating, we show that when the laser polarization is not parallel to the grating grooves the local radiation pressure can be significantly enhanced in the valleys of the grating, particularly when the grating period is close to the laser wavelength. We calculate the modified linear growth rate and the unstable wave vector spectrum which is found to depend on the laser polarization. (An independent theoretical study leading to similar conclusions has been recently reported [16].)

Our analysis is supported by particle-in-cell (PIC) simulations in two (2D) and three dimensions (3D). For circular polarization the observed hexagonal shape of RTI-generated structures resembles that predicted on the general basis of symmetry considerations. Hence, the 3D simulations provide an additional example of the recurrence of such geometry in the various contexts where the RTI plays a role, with the peculiar feature that the medium is strongly relativistic in our case. More generally this analysis provides an example of spontaneous symmetry breaking in a classical system.

II. ANALYTICAL MODEL

A. Field enhancement at a grating surface

The general problem of the reflection of an electromagnetic (EM) wave from surfaces having various modulations and arbitrary refractive index and of related phenomena, such as local field enhancement and excitation of surface waves and plasmonic modes, has a long history (see, e.g., [17]) and can be solved exactly in many cases of interest. However, for our aim it will be sufficient to consider normal incidence on perfectly reflective and shallow gratings, whose depth is small with respect to the laser wavelength, and to use a perturbative approach. We consider a plane monochromatic wave of frequency ω_0 impinging along the x direction on a perfect mirror filling the $x > x_m(y)$ region where $x_m = (\delta/2)\cos qy$ describes the sinusoidal rippling of the mirror surface [see Fig. 1(a)], with $q = 2\pi/a$, where a is the period of the ripple

*andrea.sgattoni@ino.it

†andrea.macchi@ino.it

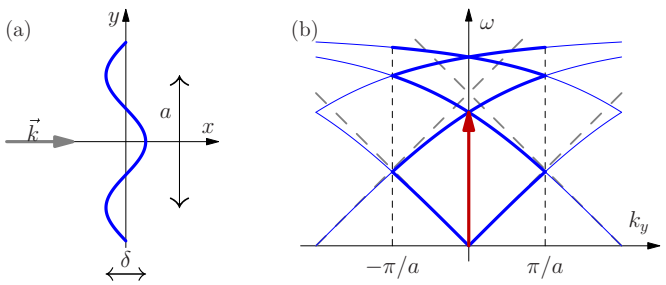

FIG. 1. (Color online) (a) The geometry used in the model calculations. (b) Phase matching between surface waves (SWs) and an EM plane wave at normal incidence on a grating. The thick lines give the dispersion relation of SWs in the (ω,k_y) plane, folded into the Brillouin zone $|k_y| < \pi/a$. The oblique dashed lines give the $\omega_p/\omega \to \infty$ limit of the SW dispersion relation. The vertical arrow represents the incident wave, i.e., $(\omega = \omega_0, k_y = 0)$.

and δ the peak-to-valley depth. Note that $y = 0$ corresponds to a valley of the rippling. Our aim is to evaluate the EM field at all points on the surface, via a perturbative approach in the small parameter $k\delta$ where $k = \omega_0/c$.

Let the electric field of the incident wave be $\mathbf{E}_i = (E_{ip}\hat{\mathbf{y}} + E_{is}\hat{\mathbf{z}})e^{ikx-i\omega_0 t}$ where $E_{ip} = E_0$ and $E_{is} = 0$ correspond to P polarization, $E_{ip} = 0$ and $E_{is} = E_0$ to S polarization, and $E_{ip} = iE_{is} = E_0/\sqrt{2}$ to circular (C) polarization. From the general solution of Helmholtz's equation, taking into account the symmetry and periodicity of the system, the components of the electric and magnetic fields along z (i.e., parallel to the grating grooves) may be written as [we omit everywhere the harmonic temporal dependence $\sim \exp(-i\omega_0 t)$]

$$E_z = E_{is}e^{ikx} - E_{rs}e^{-ikx} + \sum_{\ell=1}^{\infty} E_\ell e^{\kappa_\ell x}\cos(\ell q y), \quad (1)$$

$$B_z = E_{ip}e^{ikx} + E_{rp}e^{-ikx} + \sum_{\ell=1}^{\infty} B_\ell e^{\kappa_\ell x}\cos(\ell q y), \quad (2)$$

where $\kappa_\ell^2 = (l^2q^2 - k^2)$. Other components are simply obtained from $\mathbf{B} = -i\nabla \times \mathbf{E}/k$ and $\mathbf{E} = i\nabla \times \mathbf{B}/k$. Modes with $\ell q > k$ and κ_ℓ real are evanescent modes, while $\ell q < k$ and imaginary κ_ℓ correspond to propagating waves scattered at an angle α with respect to the normal direction such that $\tan\alpha = \ell q/|\kappa_\ell|$. For a shallow modulation we assume that E_ℓ is of order $O(k^l\delta^l)$ and we truncate the expansion (1) up to $\ell = 1$. In this case, the terms of order $O(k\delta)$ are only evanescent for $q > k$ (grating with subwavelength period) and only propagating for $q < k$. The boundary conditions at the surface are $E_z(x = x_m(y), y) = 0$, $(\mathbf{B}\cdot\hat{\mathbf{n}})(x = x_m(y), y) = 0$, and $(\mathbf{E}\times\hat{\mathbf{n}})(x = x_m(y), y) = 0$, where $\hat{\mathbf{n}} = (-\hat{\mathbf{x}} + x_m'\hat{\mathbf{y}})(1 + x_m'^2)^{1/2} \simeq -[\hat{\mathbf{x}} + \hat{\mathbf{y}}(q\delta/2)\sin qy] + O(k^2\delta^2)$ is the unit vector normal to the surface. We thus obtain $E_{rs} = E_{is}$, $E_{rp} = E_{ip}$, $E_{1x} = -i(qk\delta/\kappa_1)E_{ip}$, $E_{1y} = -ik\delta E_{ip}$, $E_{1z} = -ik\delta E_{is}$, $B_{1x} = q\delta E_{is}$, $B_{1y} = \kappa_1\delta E_{is}$, and $B_{1z} = (k^2\delta/\kappa_1)E_{ip}$.

The above relations imply that locally the field is enhanced at the peaks of the grating for S polarization and in the valleys for P polarization. To check this result we performed simulations of plane wave reflection from a reflecting, sinusoidally modulated surface using the particle-in-cell code PICCANTE (see Sec. III) at very small intensity so that only the linear response of electrons is relevant. Figure 2 shows snapshots of the cycle-averaged field from one of such simulations, where the local enhancement of the field in the grating valleys for P polarization is particularly evident.

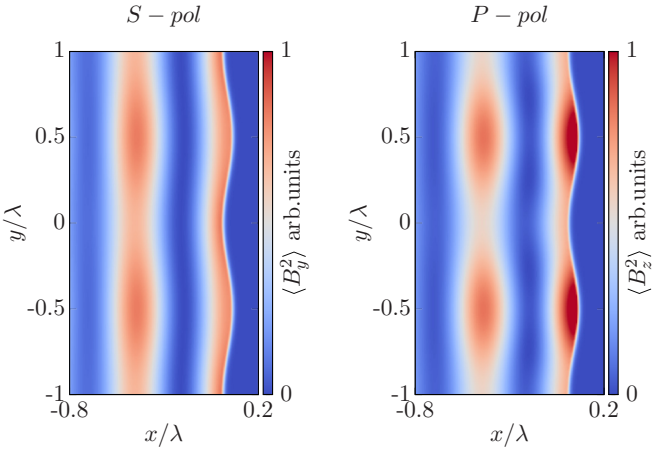

FIG. 2. (Color online) Two-dimensional simulations of plane wave reflection from a grating surface. The figures show the temporal average (over one laser period) of B_t^2, where B_t is the transverse magnetic field (in arbitrary units) for the cases of S and P polarization, i.e., for the electric field of the plane wave perpendicular and parallel to the simulation plane, respectively. For the P-polarization case, the field amplitude is locally enhanced in the valleys of the grating, while for S polarization enhancement occurs at the grating peaks.

In particular, for P polarization, in the limit $q \to k$ we have $|\kappa_1| \to 0$ and thus E_{1y} and B_{1z} diverge. This is due to the excitation of a resonant, standing surface wave (SW) in the periodic medium: in fact, because of the folding of the SW dispersion relation in the Brillouin zone $|k| < \pi/a = q/2$ [see Fig. 1(b)], there is an intersection between the dispersion curves of the EM wave at normal incidence $(k_y = 0)$ and of the SW: for a collisionless plasma and a sufficiently shallow grating, $k_y = (\omega/c)(\omega_p^2/\omega^2 - 1)^{1/2}(\omega_p^2/\omega^2 - 2)^{-1/2} \to \omega/c$ in the perfect mirror limit $\omega_p/\omega \to \infty$, with ω_p the plasma frequency; the latter case is equivalent to $q = k$, i.e., to a grating period equal to the laser wavelength. The EM wave is able to excite the SW because of the modulation, so that locally the electric field is not strictly parallel to the surface and can drive surface charge and current densities also at normal incidence. Due to the inversion symmetry, a superposition of $+q$ and $-q$ modes, i.e., a standing wave, is excited.

B. Spatial modulation of radiation pressure

We now turn to evaluate the local radiation pressure on the grating, i.e., the flow of the EM momentum through the mirror surface as a function of the position. Such flow is given by $\mathbf{P} = \mathsf{T}\cdot\hat{\mathbf{n}}$ where where $\mathsf{T}_{\alpha\beta} = (1/8\pi)[\mathrm{Re}(E_\alpha E_\beta^* + B_\alpha B_\beta^*) - \frac{1}{2}(|\mathbf{E}|^2 + |\mathbf{B}|^2)\delta_{\alpha\beta}]_{x=x_m(y)}$ is Maxwell's stress tensor evaluated at the surface and averaged over an oscillation period. For S and P polarization we obtain for the P_x component, up to

order $O(k\delta)$,

$$P_x \simeq \frac{E_0^2}{4\pi}\begin{cases}\mathrm{Re}(1-\kappa_1\delta\cos qy) & (S),\\ \mathrm{Re}\left(1+\frac{k^2}{\kappa_1}\delta\cos qy\right) & (P),\end{cases} \tag{3}$$

while $P_y \simeq (E_0^2/8\pi)q\delta\sin qy$ for both polarizations. We thus see that to first order there is no transverse modulation in P_x when $q < k$ since in this case κ_1 is an imaginary number. The modulation, to order $O(k\delta)$ occurs only for $q > k$ and it is due to the field enhancement associated with the evanescent modes.

From now on we assume $q > k$ and consider how the modulated radiation pressure may act to either smooth or enforce the surface modulation. Noting that $E_0^2/4\pi = 2I/c \equiv P_0$, i.e., the radiation pressure on a plane mirror, the local pressure due to EM momentum flow normal to the surface is

$$P_\perp = -\mathbf{P}\cdot\hat{\mathbf{n}} \simeq P_0[1+K(q)\delta\cos qy], \tag{4}$$

where $K(q) = -\kappa_1 = -(q^2-k^2)^{1/2}$ for S polarization, $K(q) = k^2/\kappa_1$ for P polarization, and $K(q) = (2k^2-q^2)/2\kappa_1$ for C polarization. Equation (4) implies that when a surface rippling occurs the radiation pressure will be modulated in the transverse direction with a different phase depending on the polarization: for P polarization $P_\perp$ locally is higher in the valleys and lower at the peaks, thus enforcing the growth of the modulation, while the opposite holds for S polarization.

C. Modified RTI growth rate

To analyze the impact of radiation pressure modulation on the RTI, we use the model of Ott [18] for the RTI of a thin foil driven by a pressure difference between the two sides. A similar extension of this model has been used in Ref. [4] to study the relativistic regime of the instability. Here for simplicity we restrict our analysis to the nonrelativistic case. We consider a thin foil of surface density σ, initially plane and placed at the position $x = 0$, with a pressure P on the $x < 0$ side. Using Lagrangian coordinates $\mathbf{r} = \mathbf{r}(\mathbf{r}_0,t)$, the equation of motion for an infinitesimal fluid element of length $d\mathbf{r} = \mathbf{r}(y_0+dy_0,t) - \mathbf{r}(y_0,t)$ and mass $dm = \sigma dy_0$ is

$$\partial_t^2\mathbf{r} = (P/\sigma)(\hat{\mathbf{x}}\partial_0 y - \hat{\mathbf{y}}\partial_0 x), \tag{5}$$

where $\partial_0 \equiv \partial/\partial y_0$. We look for an approximate solution in the form

$$x(y_0,t) \simeq \xi_0(t) + \tfrac{1}{2}\xi_x(t)e^{iqy_0} + \text{c.c.}, \tag{6}$$

$$y(y_0,t) \simeq y_0 + \tfrac{1}{2}\xi_y(t)e^{iqy_0} + \text{c.c.} \tag{7}$$

As noted in Ref. [18] such a solution is not generally sinusoidal in Eulerian variables but becomes so for small perturbations ($q|\xi_i| \ll 1$), which is consistent with our calculation of the pressure modulation. Thus we substitute for P with $P_0[1+K(q)\xi_x]$. To lowest order the equation of motion yields $\xi_0(t) = (P_0/\sigma)t^2/2$, which describes the motion of the "flat" foil. To next order the equations for ξ_x and ξ_y are

$$\partial_t^2\xi_x = (P_0/\sigma)[K(q)\xi_x + \partial_0\xi_y], \tag{8}$$

$$\partial_t^2\xi_y = -(P_0/\sigma)\partial_0\xi_x, \tag{9}$$

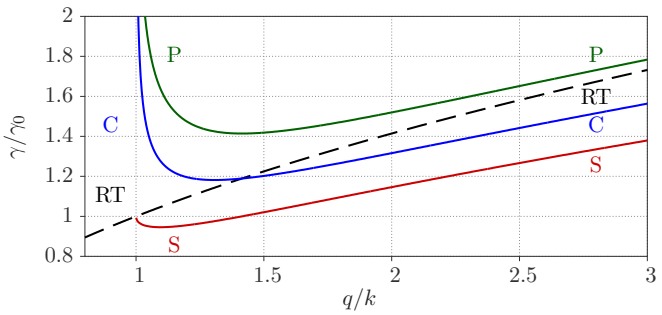

FIG. 3. (Color online) RTI growth rate of a thin foil for S, P, and circular (C) polarization. The dashed curve $\gamma_{\mathrm{RT}} = (P_0q/\sigma)^{1/2}$ gives the rate for the standard RTI of a "flat" thin foil, to which all curves are reduced for $q < k$, i.e., when κ_1 is imaginary. The parameter $\gamma_0 = (P_0k/\sigma)^{1/2}$.

which have solutions of the form $\xi_x \sim e^{\gamma t}$ and an unstable root (γ real and positive) given by

$$\gamma = (P_0/\sigma)^{1/2}\left[\left(q^2+\frac{K^2(q)}{4}\right)^{1/2}+\frac{K(q)}{2}\right]^{1/2}. \tag{10}$$

The growth rate γ is shown in Fig. 3 for the three polarizations and compared with the standard result $\gamma_{\mathrm{RT}} = (P_0q/\sigma)^{1/2}$, which still gives the growth rate for $q < k$, i.e., when there is no effect of the radiation pressure modulation and thus no polarization dependence.

Results similar to Fig. 3 are expected for thick targets because the dominant effect is the plasmonic enhancement of the field at the surface, which depends only on the period of the surface rippling. The dependence on the polarization needs a careful discussion because for high intensity the laser-plasma coupling is highly sensitive to the laser polarization. For instance, in the case of P polarization strong electron heating occurs and the surface rippling may be "washed out" by the quiver motion of the electrons. We expect the above theory to be most appropriate for circular polarization (the preferred option for radiation pressure acceleration), for which electron heating is strongly reduced and no anisotropy in the transverse plane is generated. As far as effects of higher order in $k\delta$ are of concern, we speculate that when $k\delta \sim 1$ the field may be screened into the grating valleys if $q > 2k$, similarly to what happens in a waveguide, thus reducing the RTI growth for such high-q modes.

III. SIMULATION RESULTS

A. Two-dimensional simulations

In order to test the analytical model we performed 2D PIC simulations using the PICCANTE open source code [19]. We considered a circularly polarized plane wave, irradiating a thin overdense "carbon" plasma slab (ion $Z/A = 0.5$). A periodic rippling of the foil is observed and the continuous translational symmetry is quickly broken. In Fig. 4 we show the results for a simulation performed with normalized wave amplitude $a_0 = (I/2m_ec^3n_c)^{1/2} = 66$, target thickness $d = 0.58\lambda$, and density $n_e = 37n_c$ (where n_c is the cutoff density). The transverse size of the simulation box was $L_y = 15\lambda$ and the spatial resolution $\Delta x = \Delta y = \lambda/204$.

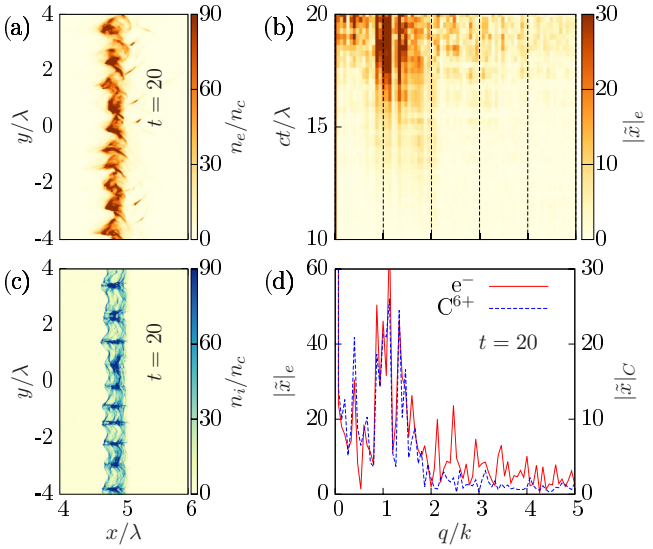

FIG. 4. (Color online) Analysis of the transverse modes in 2D plane wave simulations. (a), (c) Charge density ($t = 20\lambda/c$) of electrons and ions. For each time step the longitudinal position $x = x(y,t)$ of the vacuum-plasma interface was reconstructed as a function of the transverse coordinate y. (b) Temporal evolution of the Fourier transform $\tilde{x}(q,t)$ for electrons. (d) Comparison of $\tilde{x}$ for electrons (thick line) and carbon ions (dashed line) at $t = 20$.

A Fourier analysis of the target profile shows that the dominant modes during the onset of the instability are approximately in the range $0.8 < q/k < 2$ [Fig. 4(b)]. As expected, electrons and ions show a very similar behavior as is evident in Figs. 4(a), 4(c), and 4(d). In a very wide range of simulation parameters, we consistently observe the same behavior and a rather sharp cutoff for the modes $q > 2k$, which supports a waveguidelike screening of the field for such modes. In contrast, for linear P polarization the RTI is quenched as anticipated above.

B. Three-dimensional simulations

Large-scale 3D simulations were performed with the PIC code ALADYN [20] in the ultrarelativistic regime, for parameters close to those of Ref. [13] and of relevance for radiation pressure acceleration with the ultrahigh-intensity laser facilities under development. To save computational resources we employed a nonuniform grid in the transverse direction, i.e., a constant cell spacing is maintained in a region around the axis and then gradually stretched towards the edge. This allows us to keep a high resolution in the center and contain the expanding plasma with a feasible number of grid points. The simulation box is 93λ wide along x (the laser-propagation direction) and 120λ along y and z. In the central region ($93 \times 60 \times 60\,\lambda$) the cell size is $\Delta x = \lambda/44$, $\Delta y = \Delta z = \lambda/22$. The grid size is $4096 \times 1792 \times 1792$ cells and 64 macroparticles per cell per species are used, yielding a total number of $\simeq 2 \times 10^{10}$. The simulations were run on 16384 BlueGene/Q cores on FERMI at CINECA (Bologna, Italy). The target is composed of a first layer of ions with charge-to-mass ratio $Z/A = 1/2$ (e.g., C^{6+}), $\ell_t = \lambda$, and $n_e = 64 n_c$ (so that $\zeta = 201$), and a second layer of protons, having thickness

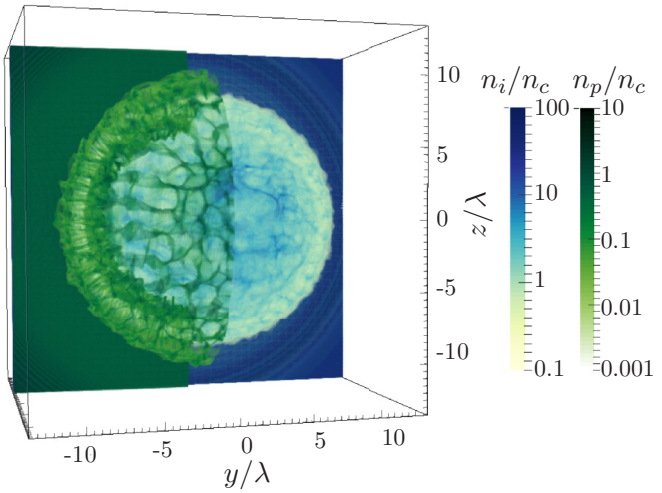

FIG. 5. (Color online) A 3D snapshot image of the density of both proton (dark green tones) and carbon (light blue tones) densities at $t = 30T$. In order to make the carbon ion density visible, the proton density is shown only on the left part ($y \geqslant 0$) of the image.

$\ell_r = \lambda/22$ and density $n_e = 8 n_c$. The laser pulse has amplitude $a_0 = 198$, a transverse Gaussian profile with waist diameter $w = 6\lambda$, and a longitudinal $\cos^2$-like profile with a full width at half maximum (FWHM) duration $\tau_p = 9\lambda/c$, all referred to the profile of the fields. Simulations have been performed using both circular (CP) and linear (LP) polarization.

Figure 5 shows a 3D ion density snapshot at an intermediate stage of the acceleration process for a simulation with optimal amplitude $a_0 = 198$ and CP. A transverse, netlike structuring of the ion density is apparent and particularly evident in the protons. In the LP case (not shown) in which $a_0 = 198\sqrt{2}$ there is a tendency of the structures to lengthen along the polarization direction.

The difference in the transverse structures between CP and LP is particularly evident for plane wave 3D simulations (performed with PICCANTE) shown in Fig. 6, where we took a uniform intensity profile and 5λ as the grid length in y and z. In the CP case we observe a pattern of hexagonal-like structures, which indeed corresponds closely to a theoretical prediction, based on symmetry arguments, for a stable structure of the flow in the nonlinear 3D development of the RTI [21]. It is

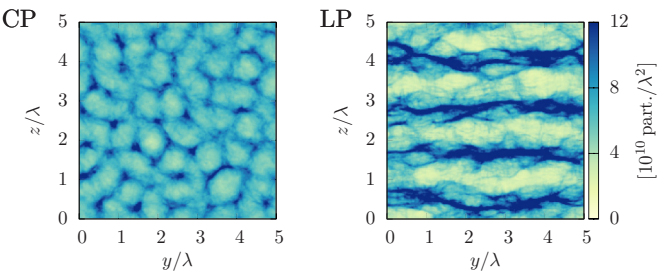

FIG. 6. (Color online) Areal density of carbon ions at $t = 15T$ in 3D simulations with the same parameters as in Fig. 5 but for a plane wave, for circular (CP) and linear (LP) polarization.

noticeable that this structure provides an example of spontaneous symmetry breaking in a classical system [22], where the continuous symmetry group of rotations and translations of the initial pulse-target system is reduced to the discrete "wallpaper" group *p6mm* [23]. For LP, the structures are strongly elongated along the polarization direction, which confirms that the laser electric field "sweeps out" the modulations. For both LP and CP, the transverse structures are visible also in the electron density (not shown) and already at $t \simeq 10T$ (a faster growth being apparent for LP).

IV. DISCUSSION AND CONCLUSIONS

The field modulation and local enhancement due to subwavelength surface rippling may play a role in other phenomena related to intense laser interaction with an overdense plasma. As an example we mention the generation of current filaments from the interaction surface, which in several simulations is correlated with a local rippling [24,25]. The transverse modulation of the field may lead to a modulation of the energies for the electrons there accelerated by the $\mathbf{v} \times \mathbf{B}$ force, providing a seed for the filamentation instability [26, and references therein] and explaining why the laser wavelength is the preferred scale for the filaments [24,27]. We also notice that the local transverse flow of momentum (P_y) at a rippled surface may lead to the generation of patterns of steady electric and magnetic fields with the ripple periodicity, which could also affect the formation of filaments.

In the context of the present work, the RTI may pose an issue for the efficiency of the light sail scheme, which is of direct interest for the development of laser-plasma ion accelerators. The early growth of the RTI does not prevent reaching high energy of ions in the radiation-pressure-dominated regime as shown in our simulation campaign [14,15], since subwavelength structures do not allow the laser pulse to be transmitted through the foil target. However, the ion beam becomes strongly modulated and nonuniform as a consequence of the RTI, and beam modulations are probably the most direct evidence of the RTI growth [10].

In conclusion, we showed that self-consistent modulation of radiation pressure and plasmonic enhancement at a rippled surface strongly affect the laser-driven Rayleigh-Taylor instability, setting a dominant scale close to the laser wavelength as observed in simulations. Three-dimensional simulations show the formation of netlike structures with approximate hexagonal wallpaper symmetry, in agreement with theoretical predictions.

ACKNOWLEDGMENTS

We thank P. Londrillo (University of Bologna and INFN, Italy) for help with the ALADYN code and M. Lupetti (Ludwig-Maximilians-Universitaet, Muenchen, Germany), F. Califano (University of Pisa, Italy), and D. Del Sarto (University of Nancy, France) for useful discussions. We acknowledge Partnership for Advanced Computing in Europe (PRACE) for access to the BlueGene/Q FERMI, based in Italy at CINECA, via the project "LSAIL." Support from Italian Ministry for education, University and Research (MIUR), Italy, via the Futuro in ricerca (FIR) project "SULDIS" is also acknowledged.

[1] S. Atzeni and J. Meyer-ter-Vehn, *The Physics of Inertial Fusion* (Oxford University Press, Oxford, 2004).
[2] See for example the Giant Hubble Mosaic image of the Crab Nebula, news release STScI-2005-37, http://hubblesite.org/newscenter/archive/releases/2005/37/.
[3] S. C. Wilks, W. L. Kruer, M. Tabak, and A. B. Langdon, Phys. Rev. Lett. **69**, 1383 (1992).
[4] F. Pegoraro and S. V. Bulanov, Phys. Rev. Lett. **99**, 065002 (2007).
[5] A. P. L. Robinson, M. Zepf, S. Kar, R. G. Evans, and C. Bellei, New J. Phys. **10**, 013021 (2008).
[6] O. Klimo, J. Psikal, J. Limpouch, and V. T. Tikhonchuk, Phys. Rev. Spec. Top.–Accel. Beams **11**, 031301 (2008); M. Chen, A. Pukhov, Z. M. Sheng, and X. Q. Yan, Phys. Plasmas **15**, 113103 (2008).
[7] M. Chen, N. Kumar, A. Pukhov, and T.-P. Yu, Phys. Plasmas **18**, 073106 (2011).
[8] V. Khudik, S. A. Yi, C. Siemon, and G. Shvets, Phys. Plasmas **21**, 013110 (2014).
[9] A. Henig *et al.*, Phys. Rev. Lett. **103**, 245003 (2009); F. Dollar *et al.*, *ibid.* **108**, 175005 (2012); I. J. Kim *et al.*, *ibid.* **111**, 165003 (2013); B. Aurand *et al.*, New J. Phys. **15**, 033031 (2013); S. Steinke *et al.*, Phys. Rev. Spec. Top.–Accel. Beams **16**, 011303 (2013); S. Kar *et al.*, Phys. Rev. Lett. **109**, 185006 (2012).
[10] C. A. J. Palmer *et al.*, Phys. Rev. Lett. **108**, 225002 (2012).
[11] H. Daido, M. Nishiuchi, and A. S. Pirozhkov, Rep. Prog. Phys. **75**, 056401 (2012); A. Macchi, M. Borghesi, and M. Passoni, Rev. Mod. Phys. **85**, 751 (2013); J. Fernández, B. Albright, F. Beg, M. Foord, B. Hegelich, J. Honrubia, M. Roth, R. Stephens, and L. Yin, Nucl. Fusion **54**, 054006 (2014).
[12] T. Esirkepov, M. Borghesi, S. V. Bulanov, G. Mourou, and T. Tajima, Phys. Rev. Lett. **92**, 175003 (2004).
[13] M. Tamburini, T. V. Liseykina, F. Pegoraro, and A. Macchi, Phys. Rev. E **85**, 016407 (2012).
[14] A. Macchi, A. Sgattoni, S. Sinigardi, M. Borghesi, and M. Passoni, Plasma Phys. Controlled Fusion **55**, 124020 (2013).
[15] A. Sgattoni, S. Sinigardi, and A. Macchi, Appl. Phys. Lett. **105**, 084105 (2014).
[16] B. Eliasson, arXiv:1408.1558.
[17] U. Fano, J. Opt. Soc. Am. **31**, 213 (1941); R. Petit, Nouv. Rev. Opt. **6**, 129 (1975); F. Toigo, A. Marvin, V. Celli, and N. R. Hill, Phys. Rev. B **15**, 5618 (1977); J. Chandezon, M. T. Dupuis, G. Cornet, and D. Maystre, J. Opt. Soc. Am. **72**, 839 (1982); M. Weber and D. L. Mills, Phys. Rev. B **27**, 2698 (1983).
[18] E. Ott, Phys. Rev. Lett. **29**, 1429 (1972).
[19] The PICCANTE code can be downloaded from the URL https://github.com/ALaDyn/piccante, doi:10.5281/zenodo.10587.
[20] C. Benedetti, A. Sgattoni, G. Turchetti, and P. Londrillo, IEEE Trans. Plasma Sci. **36**, 1790 (2008); P. Londrillo, C. Benedetti,

A. Sgattoni, and G. Turchetti, Nucl. Inst. Methods Phys. Res. A **620**, 28 (2010).
[21] S. I. Abarzhi, Phys. Rev. E **59**, 1729 (1999); Phys. Scr. **T132**, 014012 (2008).
[22] L. Michel, Rev. Mod. Phys. **52**, 617 (1980).
[23] D. Schattschneider, Am. Math. Mon. **85**, 439 (1978).
[24] Y. Sentoku, K. Mima, S.-i. Kojima, and H. Ruhl, Phys. Plasmas **7**, 689 (2000).
[25] P. Mulser, D. Bauer, S. Hain, H. Ruhl, and F. Cornolti, Laser Phys. **10**, 231 (2000).
[26] F. Califano, D. Del Sarto, and F. Pegoraro, Phys. Rev. Lett. **96**, 105008 (2006).
[27] B. F. Lasinski, A. B. Langdon, S. P. Hatchett, M. H. Key, and M. Tabak, Phys. Plasmas **6**, 2041 (1999); Y. Sentoku, K. Mima, Z. M. Sheng, P. Kaw, K. Nishihara, and K. Nishikawa, Phys. Rev. E **65**, 046408 (2002).